■ Chemical Biology

Development of Pyridazinone Chemotypes Targeting the PDEδ Prenyl Binding Site

Sandip Murarka+,[a] Pablo Martín-Gago+,[a] Carsten Schultz-Fademrecht,[b] Alaa Al Saabi,[b] Matthias Baumann,[b] Eyad Fansa,[c] Shehab Ismail,[d] Peter Nussbaumer,[b] Alfred Wittinghofer,[c] and Herbert Waldmann*[a, e]

Abstract: The K-Ras GTPase is a major target in anticancer drug discovery. However, direct interference with signaling by K-Ras has not led to clinically useful drugs yet. Correct localization and signaling by farnesylated K-Ras is regulated by the prenyl binding protein PDEδ. Interfering with binding of PDEδ to K-Ras by means of small molecules provides a novel opportunity to suppress oncogenic signaling. Here we describe the identification and structure-guided development of novel K-Ras–PDEδ inhibitor chemotypes based on pyrrolo-pyridazinones and pyrazolopyridazinones that bind to the farnesyl binding pocket of PDEδ with low nanomolar affinity. We delineate the structure–property relationship and in vivo pharmacokinetic (PK) and toxicokinetic (Tox) studies for pyrazolopyridazinone-based K-Ras–PDEδ inhibitors. These findings may inspire novel drug discovery efforts aimed at the development of drugs targeting oncogenic Ras.

Introduction

Ras proteins are key regulators of proliferation and differentiation[1,2] and are mutated in about 20–30% of human cancers, with the K-Ras isoform most frequently mutated, for example, in colon and pancreatic cancers.[3,4] Inhibition of signal transduction through the Ras-Map kinase pathway in general is considered a viable strategy for anticancer drug discovery.[5,6] However, despite substantial efforts, interference with the signal-transducing activity of the Ras proteins and their correct localization, in particular by means of farnesyltransferase inhibitors (FTIs), has not led to clinically useful drugs yet.[7–9] Recent attempts to target the Ras protein directly yielded compounds with submillimolar affinity that were inhibitors of the Ras-Sos interaction,[10–12] and covalent inhibitors of Ras signaling that target the G12C mutation in K-Ras which occurs with high frequency in lung cancer.[13–15]

The biological function of Ras proteins critically depends on their correct subcellular localization, which in turn is regulated by lipid modifications at their C terminus.[16,17] K-Ras, the major oncogenic isoform of the Ras proteins carries a C-terminal S-farnesylated cysteine methyl ester. Recently it was demonstrated that the prenyl binding protein PDEδ binds K-Ras and the Ras homologue RheB through the farnesylated carboxymethylated C terminus,[18–20] sustains their spatial organization and proper localization in cells, and critically regulates signaling of oncogenic K-Ras.[19,21] Along these lines, we showed that interference with the K-Ras–PDEδ interaction with the small molecule inhibitor Deltarasin **1a** (Figure 1) inhibits oncogenic Ras signaling in cells and blocks proliferation of human pancreatic ductal adenocarcinoma (hPDAC) cells harboring oncogenic K-Ras in vitro and in vivo.[22]

However, despite the fact that Deltarasin binds the prenyl binding pocket of PDEδ with nanomolar affinity in vitro, growth inhibition requires micromolar concentrations of the compound, raising the question whether this observation is chemotype-dependent or rather reflects the influence of an underlying biological mechanism, which would be of utmost importance for any further inhibitor development. To this end, we recently documented the discovery of pyrazolopyridazinone-based, highly selective PDEδ inhibitors that exhibit less unspecific cytotoxicity than the previously reported Deltarasin **1a** and demonstrate a high correlation with the phenotypic effect of PDEδ knockdown in a set of human pancreatic cancer cell lines.[23]

Here we describe the identification and structure-guided development of novel K-Ras–PDEδ inhibitor chemotypes featuring pyrrolopyridazinones and pyrazolopyridazinones that bind

[a] *Dr. S. Murarka,+ Dr. P. Martín-Gago,+ Prof. Dr. H. Waldmann*
    Max-Planck-Institut für Molekulare Physiologie
    Abteilung Chemische Biologie, Otto-Hahn-Straße 11
    44227 Dortmund (Germany)
    E-mail: herbert.waldmann@mpi-dortmund.mpg.de

[b] *Dr. C. Schultz-Fademrecht, Dr. A. Al Saabi, Dr. M. Baumann,*
    Dr. P. Nussbaumer
    Lead Discovery Center GmbH, 44227 Dortmund (Germany)

[c] *Dr. E. Fansa, Prof. Dr. A. Wittinghofer*
    Max-Planck-Institut für Molekulare Physiologie
    Structural Biology Group, 44227 Dortmund (Germany)

[d] *Dr. S. Ismail*
    Beatson Institute for Cancer Research, Bearsden, Glasgow G61 1BD (UK)

[e] *Prof. Dr. H. Waldmann*
    Technische Universität Dortmund, Fakultät Chemie
    Chemische Biologie, Otto-Hahn-Straße 6, 44221 Dortmund (Germany)

[+] *These authors contributed equally to this work.*

⌨ *Supporting information for this article is available on the WWW under http://dx.doi.org/10.1002/chem.201603222.*
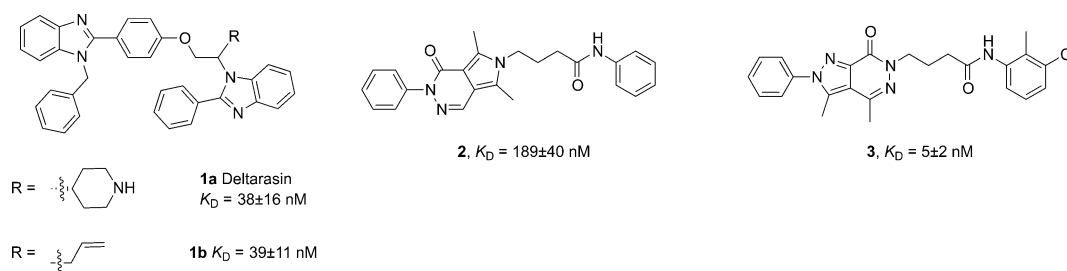
Figure 1. Bisbenzimidazole-based inhibitors **1a** (Deltarasin) and **1b** and novel inhibitor chemotypes pyrrolopyridazinone **2** and pyrazolopyridazinone **3** identified through alpha screen.

to the farnesyl-binding hydrophobic pocket of PDEδ with low nanomolar affinity. We detail the synthesis of these PDEδ inhibitor classes, and report the structure–property relationship study for pyrazolopyridazinone-based K-Ras–PDEδ inhibitors with a view to identify a suitable candidate for in vivo studies. We report in vivo pharmacokinetic (PK) and toxicokinetic (Tox) studies using a set of inhibitors based on the pyrazolopyridazinone scaffold.

Results and Discussion

Our previously developed biophysical alpha screen assay[22] was employed to search for alternative chemotypes that can be evolved into individual inhibitors with a potency similar to Deltarasin **1a**. The screen revealed pyrrolopyridazinone **2** and pyrazolopyridazinone **3** as inhibitors of the K-Ras–PDEδ interaction (Figure 1). High inhibitory potency in vitro was independently confirmed by means of a fluorescence polarization assay as described previously.[22]

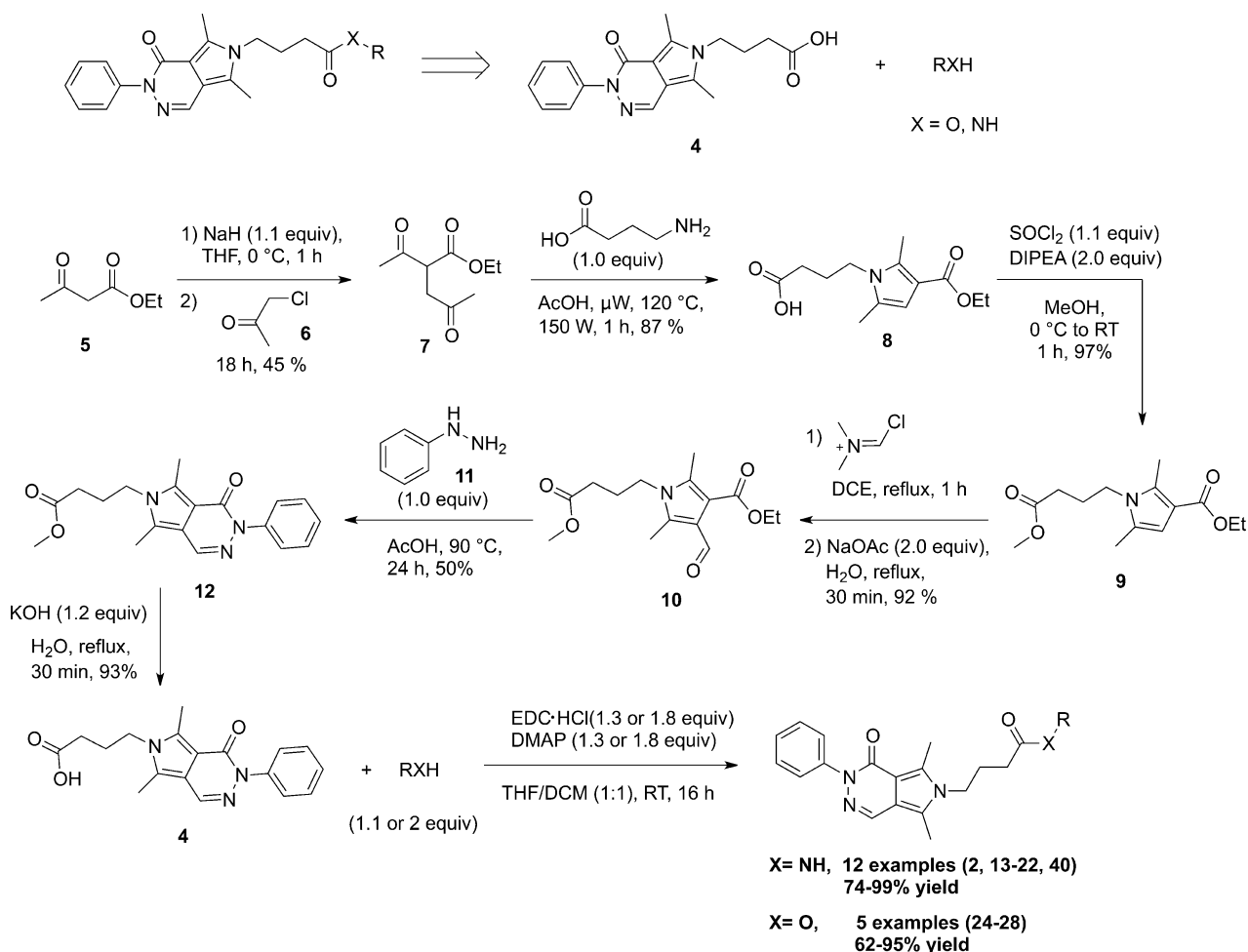### Development of pyrrolopyridazinone inhibitors

Since the initial hit based on the pyrrolopyridazinone scaffold embodied an anilide functionality, we decided to prepare a collection of structurally and electronically diverse anilide derivatives and their corresponding bioisosteric ester analogues. The targeted pyrrolopyridazinone-based amides and esters were retrosynthetically disconnected to the carboxylic acid precursor **4** and corresponding amines or alcohols, which can be linked by standard coupling methods (Scheme 1). The synthesis of acid fragment **4** commenced with commercially available **5**, which was treated with **6** in the presence of sodium hydride to afford tricarbonyl derivative **7** in 45% yield (Scheme 1). Subsequent heating of **7** and 4-aminobutanoic acid in acetic acid under microwave conditions at 120 °C yielded pyrrole derivative **8** in 87% yield. The free acid in **8** was then esterified by using thionyl chloride and MeOH yielding **9** in 97% yield. Subsequently, ester **9** was subjected to Vilsmeier–Haack formylation to give aldehyde **10**, which was then condensed with phenyl hydrazine in acetic acid to form pyridazinone **12** in 93% yield. Finally, saponification of **12** gave the final acid precursor **4** in excellent yield. With acid **4** in hand, a range of amides (**2**, **13–22**, **40**) and esters (**24–28**) were synthesized in good yields (62–99%) at ambient temperature using 1-ethyl-3-

(3-dimethylaminopropyl)carbodiimide (EDC) as the coupling reagent.

The binding efficacy of the synthesized analogues was evaluated by means of a fluorescence polarization assay based on a known PDEδ ligand. Our results show that introduction of a methyl substituent on the phenyl ring of the amide functionality leads to a two- to threefold increase of binding potency (Table 1, entries 1–3). Whereas, ortho- and para-substitution imparted similar effects, meta-dimethyl substituted anilides proved to be slightly less effective (entries 2–4). Electron-withdrawing substituents on the phenyl ring showed marginal effects as compared to unsubstituted or methyl-substituted analogues (entries 9–11). Replacement of the methyl substituent with an electron-rich methoxy functionality yielded much higher K_D values irrespective of the substitution pattern. The additional increase of electron density turned out to be detrimental (entries 5–8). Importantly, a benzyl amide demonstrated a similar level of potency as compared to methyl-substituted anilide derivatives (entry 12). We then sought to explore the efficacy of bioisteric ester analogues as they can impart interesting effects owing to their rigidity, different hydrogen-bonding properties and conformational orientation. None of the tested phenyl ester analogues showed potency higher than the corresponding amide congener (entries 13–16) and by analogy a benzyl ester showed potency similar to methyl-substituted phenyl ester derivatives (entry 17). Considering the fact that the benzyl amide showed slightly higher binding affinity and since they are stable to cleavage by hydrolases in prospective cellular investigations we decided to further investigate this chemotype.

Since initial attempts to obtain a crystal structure of pyrrolopyridazinone **23** and close analogues in complex with PDEδ failed, molecular modeling (Schrödinger, Maestro suite) was employed to predict the binding mode of **23** for optimization of binding and potency. Our docking studies suggest that **23** binds deeply in the hydrophobic tunnel of PDEδ with H-bonding to Tyr149 and Arg61 (Figure 2). This binding mode closely resembles the interactions of Deltarasin analogue **1b** with PDEδ (Figure 2).[22]

Based on these results and since modeling also suggested that substituents on the N-phenyl ring would clash with the protein, the length of the linker between the two hydrogen-bonding groups and the structure of the amide were varied. Determination of K_D values in fluorescence polarization assays

⬉⬉ These are not the final page numbers!

Scheme 1. Synthesis of pyrrolopyridazinone-based amide (**2**, **13–22**, **40**) and ester (**24–28**) derivatives.
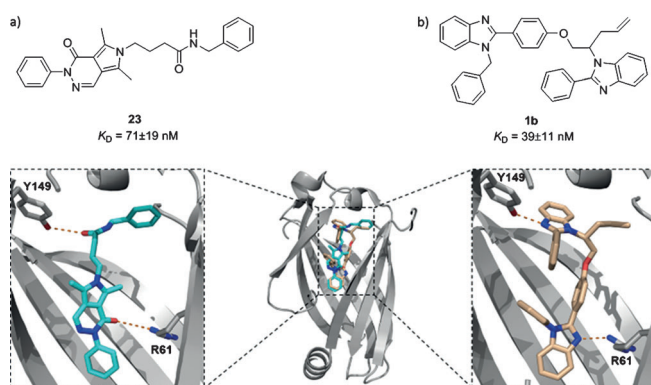

Figure 2. Comparison between the binding mode of inhibitors **23** and **1b**. a) Modeling (Schrödinger, Maestro suite) of **23**. b) Crystal structure of inhibitor **1b** in complex with PDEδ showing H-bonding interactions with the same amino acids, Tyr149 and Arg61, respectively, as predicted for inhibitor **23**. A graphic of **1b** in complex with PDEδ highlighting the surface of the pocket can be found in the Supporting Information, Figure S4.

revealed that introduction of a chlorine atom into the phenyl ring results in an increased potency whereas a methoxy substituent is less advantageous (Table 2, entries 2–5). Importantly,

reducing the linker length drastically diminished the binding affinity (compare entries 2 vs. 6 and 4 vs. 7). Shortening of the linker does probably not allow H-bond formation between the amide carbonyl and Tyr149. Replacement of the benzyl amide phenyl ring by different electron-rich or electron-poor heterocycles led to substantially higher K_D values (entries 8–10). However, cycloalkylamides with alkyl groups of similar size as the phenyl ring were potent inhibitors (Table 1, entries 13–16). Substituted cylohexyl amide derived inhibitors bind to PDEδ with low nanomolar affinity (entries 13–16) presumably due to hydrophobic interactions which increase with the ring size.

In an attempt to further improve the drug-like properties and explore an isosteric[24] replacement of the amide group, a series of 1,2,4- and 1,3,4-oxadiazoles **45–50** and **52–58** was investigated (Scheme 2). The two-step one-pot synthesis of 1,2,4-oxadiazoles **45–50** was accomplished in good yields (55–60%) by treating acid precursor **4** with the corresponding amidoxime derivatives **44** in the presence of EDC·HCl in diglyme, followed by heating to 110°C for the cyclodehydration step.[25] Similarly, 1,3,4-oxadiazoles **52–58** were obtained in 58–80% yields by treatment of **4** with benzoylhydrazides **51** in the presence of N,N,N',N'-tetramethyl-O-(1H-benzotriazol-1-yl)uronium hexafluorophosphate (HBTU) and subsequent ring closure

Table 1. K_D values for pyrrolopyridazinone-based anilides and esters as determined by fluorescence polarization experiments.
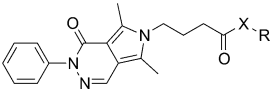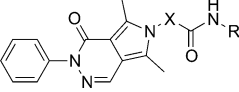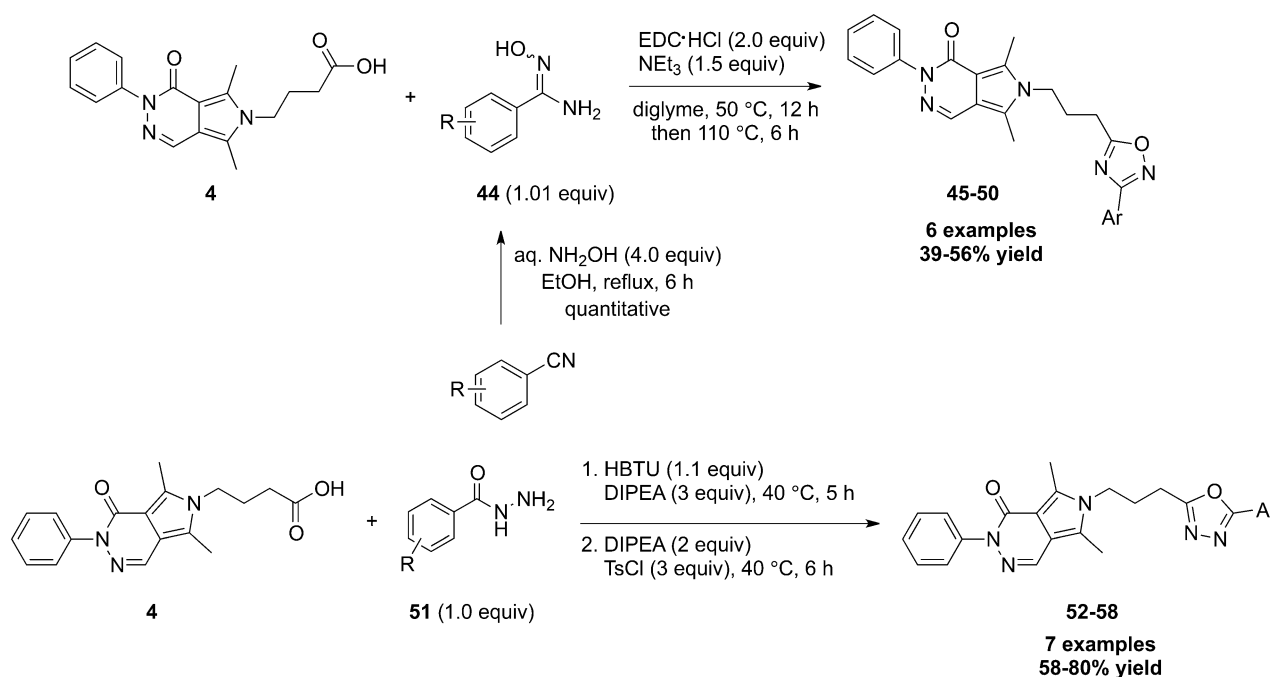

Entry	Nr.	X	R	K_D [nM]	Entry	Nr.	X	R	K_D [nM]
1	**2**	NH	phenyl	189 ± 40	10	**21**	NH	2,4-difluorophenyl	83 ± 24
2	**13**	NH	2-methylphenyl	74 ± 19	11	**22**	NH	2-methyl-4-chlorophenyl	96 ± 31
3	**14**	NH	4-methylphenyl	74 ± 17	12	**23**	NH	benzyl	71 ± 19
4	**15**	NH	3,5-dimethylphenyl	134 ± 34	13	**24**	O	phenyl	242 ± 35
5	**16**	NH	2-methoxyphenyl	243 ± 43	14	**25**	O	2,4-dimethylphenyl	163 ± 24
6	**17**	NH	4-methoxyphenyl	282 ± 52	15	**26**	O	2,5-dimethylphenyl	265 ± 28
7	**18**	NH	benzo[d][1,3]dioxol-5-yl	93 ± 21	16	**27**	O	3-methoxyphenyl	614 ± 70
8	**19**	NH	3,4,5-trimethoxyphenyl	$> 10^3$	17	**28**	O	benzyl	250 ± 51
9	**20**	NH	4-fluorophenyl	133 ± 30					

Table 2. K_D values for pyrrolopyridazinones with different linker and amide structure as determined by fluorescence polarization measurements.

Entry	Nr.	X	R	K_D [nM]	Entry	Nr.	X	R	K_D [nM]
1	**23**	$-(CH_2)_3-$	benzyl	71 ± 9	9	**36**	$-(CH_2)_3-$	furan-2-ylmethyl	428 ± 80
2	**29**	$-(CH_2)_3-$	3-methoxybenzyl	119 ± 30	10	**37**	$-(CH_2)_3-$	pyridin-2-ylmethyl	815 ± 118
3	**30**	$-(CH_2)_3-$	3-chlorobenzyl	41 ± 5	11	**38**	$-(CH_2)_3-$	cyclopropyl	634 ± 56
4	**31**	$-(CH_2)_3-$	2-chlorobenzyl	32 ± 11	12	**39**	$-(CH_2)_3-$	cyclopentyl	102 ± 19
5	**32**	$-(CH_2)_3-$	4-chlorobenzyl	58 ± 13	13	**40**	$-(CH_2)_3-$	cyclohexyl	23 ± 3
6	**33**	$-CH_2-$	3-methoxybenzyl	$> 10^3$	14	**41**	$-(CH_2)_3-$	4-methylcyclohexyl	29 ± 5
7	**34**	$-CH(Me)-$	2-chlorobenzyl	$> 10^3$	15	**42**	$-(CH_2)_3-$	2-methylcyclohexyl	22 ± 4
8	**35**	$-(CH_2)_3-$	thiophen-2-ylmethyl	132 ± 9	16	**43**	$-(CH_2)_3-$	3-methylcyclohexyl	15 ± 6

↖↖ These are not the final page numbers!

Scheme 2. Synthesis of 1,2,4- (**45**–**50**) and 1,3,4- (**52**–**58**) oxadiazole derivatives.

mediated by 4-methylbenzenesulfonyl chloride (TsCl) and diiso-propylethylamine (DIPEA).[26]

K_D value determination for these heterocycles revealed that none of these isosteres reached the potency of the guiding amides (Table 3). However, we were able to co-crystallize the 1,3,4-oxadiazole **52** in complex with PDEδ (2.1 Å resolution, Figure 3a and c). Close analysis revealed that binding is mediated by hydrophobic interactions and two H-bonds between the carbonyl group of the pyridazinone and Arg61, and between the oxadiazole and Tyr149. These results validate the guiding docking experiments described above. Further design based on the co-crystal structure of **52** with PDEδ suggested the additional filling of the empty space in the hydrophobic pocket of PDEδ (Figure 3d). To meet this goal and in order to retain the H-bond to Tyr149, N-alkylated benzimidazole **61** was introduced (Figure 3b and e). Benzimidazole fragment **60** was synthesized by a condensation reaction between acid **4** and commercially available phenylenediamine **59** using polyphosphoric acid (Scheme 3). The intermediate **60** was either N-alkylated by using benzylbromide to obtain **61** or was modified by Mitsunobu reaction using n-tributylphosphine and tetramethylazadicarboxamide (TMAD) to deliver thiophenylated fragment **62** (Scheme 3).

Gratifyingly, the newly designed chemotypes, **61** and **62**, emerged as highly potent inhibitors that bind to PDEδ with very low nanomolar affinities ($K_D < 5$ nM), supporting the structural model (Figure 3e).

Development of pyrazolopyridazinone inhibitors

Structure-based development of the pyrazolopyridazinone hit class was enabled by a crystal structure of inhibitor **3** in com-

Table 3. K_D values for 1,2,4- (**45**–**50**) and 1,3,4- (**52**–**58**) oxadiazole derivatives.

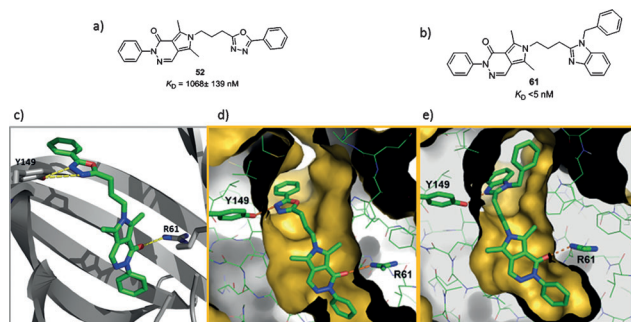| Entry	Nr.	Ar	K_D [nM]
1	45	–phenyl	758 ± 155
2	46	–4-methylphenyl	1036 ± 212
3	47	–4-OMe-phenyl	1072 ± 249
4	48	–3,5-diOMe-phenyl	3039 ± 964
5	49	–4-CF₃-phenyl	1389 ± 374
6	50	–4-F-phenyl	830 ± 249
7	52	–phenyl	1068 ± 139
8	53	–4-methylphenyl	1372 ± 273
9	54	–4-OMe-phenyl	1368 ± 307
10	55	–3-OMe-phenyl	550 ± 53
11	56	–4-CF₃-phenyl	1072 ± 233
12	57	–4-F-phenyl	947 ± 182
13	58	–pyridyl	2326 ± 682

Figure 3. Development of pyrrolopyridazinone-based inhibitors with isosteric amide group replacements. Structure and binding affinities (competitive fluorescence polarization assay, see the Supporting Information) of: a) compound **52**, and b) compound **61**. c) Crystal structure of inhibitor **52** in complex with PDEδ at 2.10 Å resolution. d) Surface representation of PDEδ and overlay of oxadiazole **52** showing an empty space in the hydrophobic tunnel. e) Surface representation of the PDEδ structure and fitting of the designed N-benzylated benzimidazole derivative **61** in the hydrophobic tunnel. Tyr149 (Y149) and Arg61 (R61) are shown as sticks to highlight the hydrogen-bond interactions.

plex with PDEδ (Figure 3 a and c, 2.6 Å) which revealed that heterocycle **3** also employs H-bonds to Tyr149 and Arg61 for binding. Since the binding mode of inhibitor **3** is analogous to binding of inhibitor **52**, a C3-linker was kept for further optimization of affinity. Considering that anilides are not desired in medicinal chemistry investigations and since modeling indicated that benzyl amides could adopt a conformation in which a simultaneous H-bond with Tyr149 could be formed and the

empty space in the PDEδ pocket could be filled, a series of this chemotype was investigated.

In analogy to the disconnection of the pyrrolopyridazinone scaffold, amides based on the pyrazolopyridazinone core were synthesized by coupling acid precursor **72** with the corresponding amine derivatives in the presence of EDC as the coupling reagent (Scheme 4). The acid **72** was synthesized in six linear steps starting from commercially available aniline derivatives **63**. The hydrazonyl chloride **66** was synthesized through the Japp–Klingemann reaction by treating **65** with benzene diazonium derivative **64** that was generated in situ from the aniline derivative **63** (Scheme 4).[27] The pyrazole core **68** was constructed by mixing hydrazonyl chloride **66** with a solution of enolate **67** at ambient temperature.[27] Following this procedure, refluxing pyrazole **68** with hydrazine in ethanol afforded pyrazolopyridazinone **69**,[26] which was alkylated with methyl 4-bromobutanoate (**70**) to give **71** in good yield. Subsequently, **71** was hydrolyzed to obtain the corresponding acid precursor **72**.

Indeed, benzyl amide **74** binds to PDEδ with nanomolar affinity (Table 4, entry 3). Ring-size reduction (Table 4, entry 2) or incorporation of a substituent on the phenyl ring was not favorable (Table 4, entries 4–7). Homobenzyl amides also proved to be potent inhibitors (entries 8 and 9). Our modeling studies suggested that a small substituent might be attached to the N-phenyl moiety pointing deep into the farnesyl binding site. As we expected, incorporation of a p-methyl substituent into the pyrazole N-phenyl ring resulted in low nanomolar affinity (Table 4, entries 2–4 and 7–9 vs. 10, 14–16, 18, 19). Additional
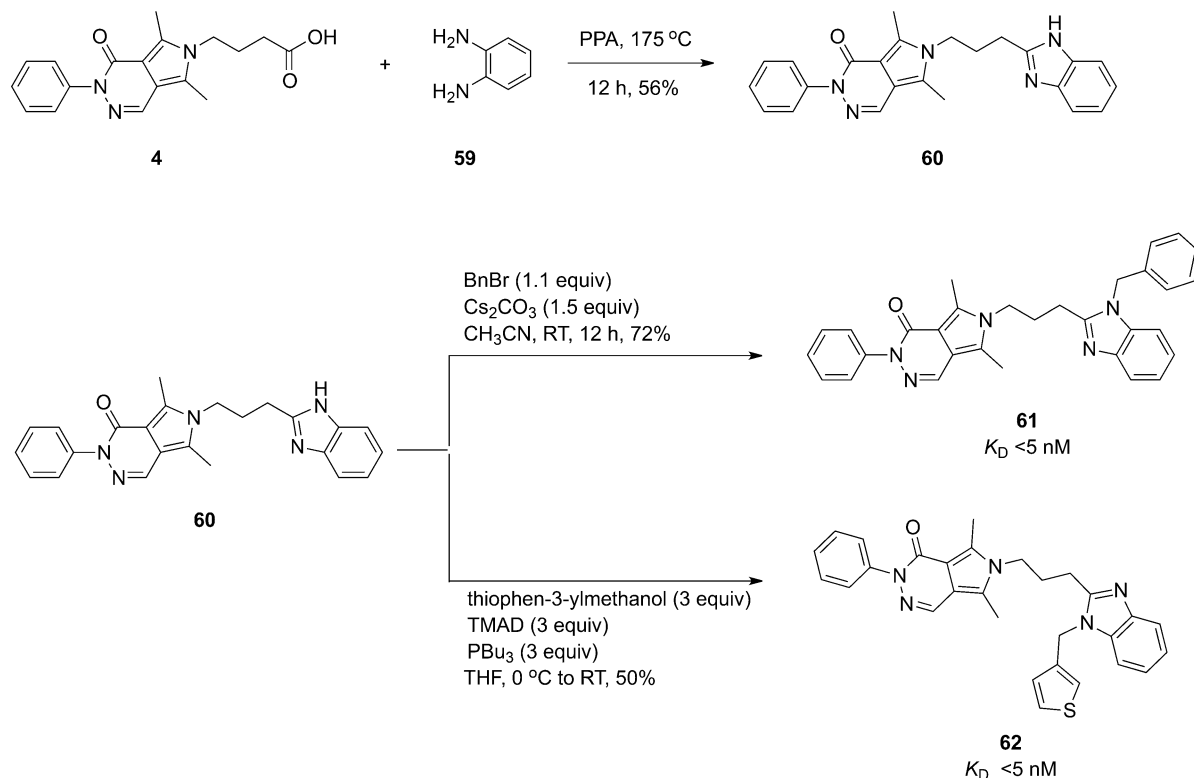
Scheme 3. Synthesis of N-alkylated benzimidazole derivatives **61** and **62** and their binding affinities as measured by fluorescence polarization.

↖↖ **These are not the final page numbers!**
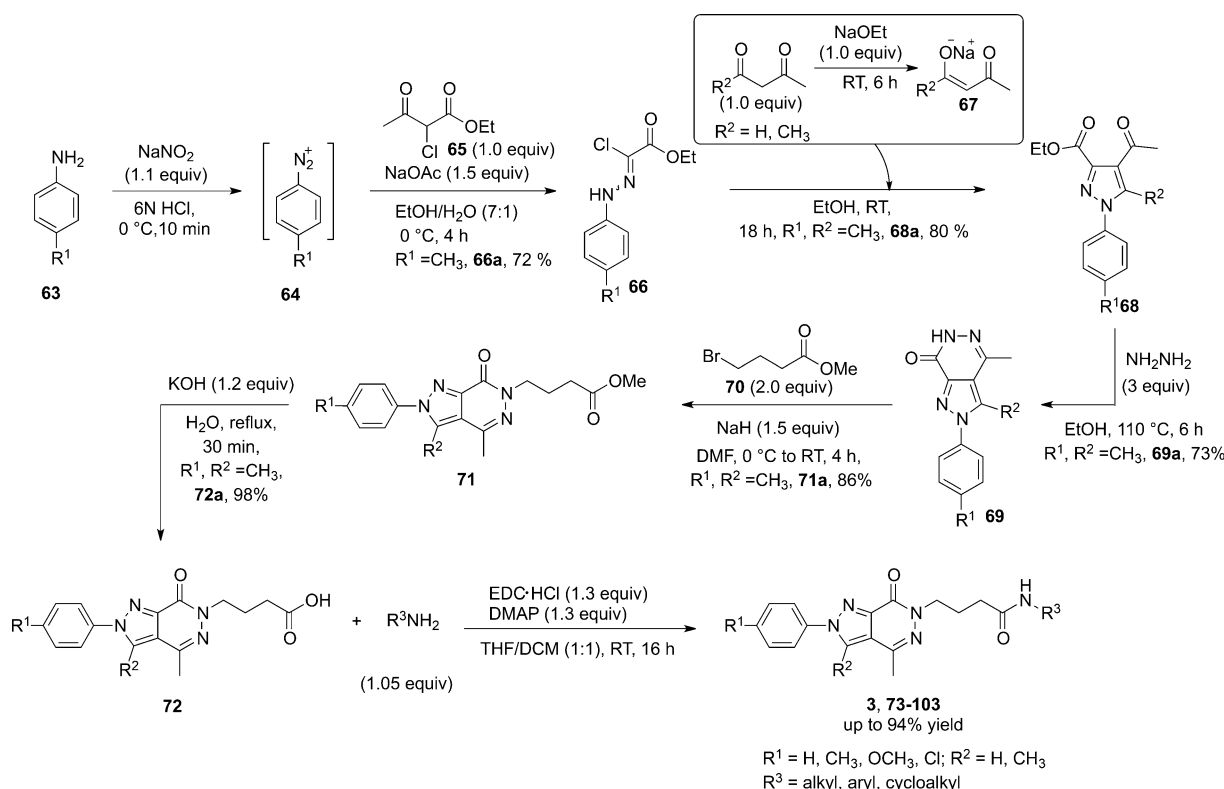
Scheme 4. Synthesis of pyrazolopyridazinone-derived amide (**3**, **73**–**96**) derivatives.

replacement of the benzyl amide by a smaller furyl-, a tetrahydrofuryl group or a pyridine was not favorable (entries 10–13). Interestingly, *para*-methyl and *para*-isopropoxy substituted benzylamides (entries 16 and 17) as well as several homobenzyl amides displayed low nanomolar affinities, regardless of the substitution pattern on the phenyl backbone (entries 18–22). Notably, cycloaliphatic amides proved to be potent inhibitors with the activity dependent on their ring-sizes (entries 23–25).

While very potent molecules were identified, ligand efficiency, solubility, and drug likeness of the compounds still left room for further optimization.[28] Compound **93** was selected for further optimization, because we assumed that the presence of an additional methyl group at the benzylic position in **93** would further stabilize the compound against metabolic degradation. Furthermore, molecular modeling experiments indicated that **93** will form the same hydrogen bonds as **3** and may additionally form a hydrogen bond with glutamine-78 (Figure 4 d). Based on this reasoning, **93** was subjected to a panel of biochemical and pharmacological screens in order to determine its selectivity profile and possible interactions with other pharmacologically relevant proteins.[23] This compound proved to be remarkably selective as compared to Deltarasin and was chosen for further development (Supporting Information, Figure S1).[23]

In vitro, **93** revealed an acceptable early ADME (eADME) profile with the exception of high instability in the presence of mouse liver microsomes (Table 5, entry 1 and Table S1 in the Supporting Information). Non-quantitative in silico prediction of the most liable sites of **93** pointed at four metabolic hot-
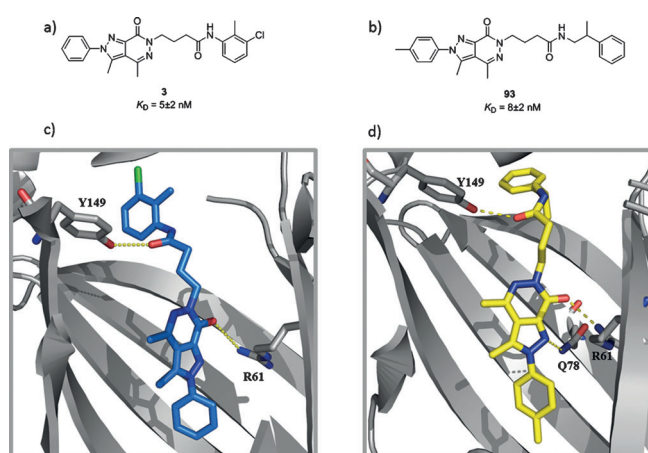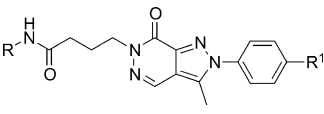

Figure 4. Identification of pyrazolopyridazinone-based K-Ras–PDEδ inhibitor chemotype. Structure and binding affinities (competitive fluorescence polarization assay, see the Supporting Information) of: a) pyrazolopyridazinone derivative **3**, and b) **93**. c) Crystal structure of inhibitor **3** in complex with PDEδ at 2.60 Å resolution. Tyr149 (Y149) and Arg61 (R61) are shown as sticks to highlight the hydrogen-bond interactions. d) Predicted binding mode of **93** (best docking pose; Schrödinger, Maestro suite). Besides Y149 and R61, Gln78 (Q78) is also shown as stick to highlight the probable third H-bond interaction. A graphic of **93** docked into PDEδ highlighting the surface of the pocket can be found in the Supporting Information, Figure S4.

spots that are likely prone to CYP450-mediated metabolism (Supporting Information, Figure S2). Consistent with the in silico prediction, we confirmed experimentally that these positions are attacked by CYP enzymes in mouse liver microsomes

Table 4. K_D values for pyrazolopyridazinones with different amide structures and *N*-phenyl substituents, as determined by fluorescence polarization measurements.

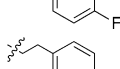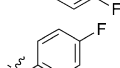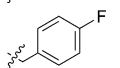| Entry	Nr.	R¹	R	K_D [nм]	Entry	Nr.	R¹	R	K_D [nм]
1	**3**	H	2-chloro-6-methylphenyl	5±2	13	**84**	CH₃	pyridin-3-ylmethyl	149±18
2	**73**	H	furan-2-ylmethyl	136±55	14	**85**	CH₃	benzyl	17±9
3	**74**	H	benzyl	42±15	15	**86**	CH₃	4-methylbenzyl	6±2
4	**75**	H	4-methoxybenzyl	81±21	16	**87**	CH₃	4-methoxybenzyl	18±6
5	**76**	H	3-methoxybenzyl	99±15	17	**88**	CH₃	4-isopropoxybenzyl	8±3
6	**77**	H	2-methoxybenzyl	95±18	18	**89**	CH₃	phenethyl	6±2
7	**78**	H	4-methylbenzyl	96±14	19	**90**	CH₃	4-methylphenethyl	5±3
8	**79**	H	phenethyl	29±7	20	**91**	CH₃	4-chlorophenethyl	6±2
9	**80**	H	4-methylphenethyl	19±6	21	**92**	CH₃	2-chlorophenethyl	5±2
10	**81**	CH₃	furan-2-ylmethyl	50±16	22	**93**	CH₃	1-phenylethyl	8±4[a]
11	**82**	CH₃	tetrahydrofuran-2-ylmethyl	56±6	23	**94**	CH₃	cyclopropyl	258±18
12	**83**	CH₃	pyridin-2-ylmethyl	178±30	24	**95**	CH₃	cyclobutylmethyl	13±3
					25	**96**	CH₃	4-methylcyclohexyl	5±1

[a] (*S*)-**93** $K_D = 5(\pm 3)$ нм; (*R*)-**93** $K_D = 12(\pm 4)$ нм.
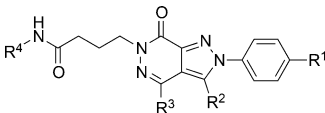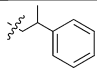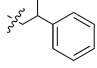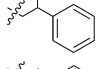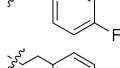
(Supporting Information, Figure S3). These studies also showed that a variety of additional metabolites were formed by CYP450-mediated metabolism in vitro. In a next step we performed a structure–property relationship (SPR) study focusing on improving the metabolic stability of **93** in order to identify a suitable in vivo candidate.

We first removed the methyl group on the eastern phenyl 4-position that was identified as one of the metabolic sites for degradation. The modification proved to be inefficient both in terms of affinity and clearance, which in turn demonstrates the importance of the methyl functionality (Table 5, entry 2). Keeping the other functionalities intact, removal of the methyl functionality on the central pyrazole ring drastically improved the clearance, while potency remained unchanged (entry 3). This result shows that this site is indeed highly susceptible towards metabolic degradation and corroborated the in silico prediction. Then we sought to investigate the metabolic hot-spots on the remaining part of the molecule and accordingly, the benzylic methyl functionality was removed and the 4-position

of the phenyl ring was blocked with a fluorine atom (entry 4). The metabolic stability of the corresponding compound increased substantially, while similar K_D values were obtained (entry 4). Comparable levels of potency and metabolic stability were observed when the methyl group on the phenyl 4-position was replaced with a chloro functionality for the fluorinated homobenzyl derivatives (entry 5). Replacement of chloro/methyl substituents with electron-rich methoxy groups drastically diminished the metabolic stability of the molecule **103** without altering the binding affinity (entry 6). It is important to mention that fluorinated benzyl amide analogues containing a methyl- or chloro- moiety (**102**, **103**) on the phenyl ring showed high metabolic stability in mouse liver microsomes (entries 7 and 8). Compound **99** was found to be kinetically more soluble as compared to **100** and hence was chosen for in vivo pharmacokinetic (PK) and toxicokinetic (Tox) studies to eventually find a suitable route of administration and a maximum tolerated dose to guide efficacy experiments in mouse models of xenografted K-Ras-dependent and K-Ras-independ-

Table 5. K_D, IC$_{50}$ value in PaTu8902/Panc1 CTG assay, kinetic solubility and clearance values for pyrazolopyridazinones.

Entry	Nr.	R^1	R^2	R^3	R^4	K_D [nM]	PaTu8902/Panc1 CTG IC$_{50}$ [µM]	SolRank [µM]	Clint, mouse [µL min^{-1} mg^{-1}]
1	**93**	CH$_3$	CH3	CH$_3$	(1-phenylethyl)	8±4	12.5/>30	49.7	1746
2	**97**	H	CH3	CH$_3$	(1-phenylethyl)	22±6	13.5/n.d.	364.1	1980
3	**98**	CH$_3$	H	CH$_3$	(1-phenylethyl)	6±3	4.7/n.d.	83.6	447
4	**99**	CH$_3$	H	CH$_3$	(4-fluorobenzyl)	8±4	12.3/n.d.	99.9	40
5	**100**	Cl	H	CH$_3$	(4-fluorobenzyl)	10±5	14.3/n.d.	20.3	27
6	**101**	H$_3$CO	H	CH$_3$	(4-fluorobenzyl)	6±3	n.d.	21.9	1260
7	**102**	CH$_3$	H	CH$_3$	(3-fluorophenyl)	129±22	n.d.	8.7	29
8	**103**	Cl	H	CH$_3$	(3-fluorobenzyl)	125±16	>30/>30	1.6	10

ent PDAC cell lines (see Supporting Information Table S1 for ADME profile of **99** and **100**). Deltarasin showed a kinetic solubility of 270 µM in the same SolRank assay.

Different vehicles (A = 5% Tween-80, 50% NaCl, 45% H$_2$O; B = 20% DMSO, 80% PEG200; C = 15% DMSO, 9.5% Cremophor EL/EtOH (1:1), 75.5% H$_2$O) were used to generate suitable compound formulations for oral and intraperitoneal (IP) dosing. Whereas only very low compound levels were found in plasma after oral dosage (data not shown), significantly higher plasma concentrations were found after IP administration of **99** in vehicle A, B or C at 10 mg kg^{-1} (Figure 5 a). However, at this dose no major improvement of the plasma concentration/time curves of **99** compared to **93** was observed. Nevertheless, as slightly higher compound levels were measured for **99** with vehicle B during the terminal phase, the DMSO/PEG formulation was chosen for further studies. Surprisingly, when the IP dose was increased to 30 mg kg^{-1} in DMSO/PEG, serious adverse effects, such as hard breathing, crouching and low blood pressure, emerged within minutes after the administration (data not shown). Similar toxic side effects were observed for **93**, although previously it was found to be well tolerated at up to 250 mg kg^{-1} when formulated in vehicle A. Although, IP application of **99** at a dose of 30 mg kg^{-1} in vehicle A was well tolerated, it did not lead to an increase of the plasma exposure in comparison to **93** (Figure 5 b).

Next, we investigated intravenous dosing with formulation 10% DMSO, 90% serum. Indeed, a significant increase of the plasma exposure as well as the terminal half-life was observed for **99** in comparison to **93** after intravenous (IV) dosing in mice (Figure 6).

Attempts to develop a covalent inhibitor

Covalent drugs have witnessed resurgence in recent years.[29] The design of selective covalent inhibitors is conceptually highly attractive and requires a right balance between reactivity and selectivity. Selective irreversible covalent binding of an inhibitor to the target of interest often displays increased biochemical efficiency and high residence time compared to reversible binding, and hence the desired pharmacological effect is achieved at lower drug concentrations. We therefore investigated the possibility of irreversible inhibition of PDEδ by forming a covalent bond between a Michael acceptor and a cysteine residue. Since PDEδ features only one cysteine close to the hydrophobic farnesyl binding cavity (Cys56, Figure 7 a), pyrrolo- and pyrazolopyridazinone-based reversible inhibitors were equipped with reactive Michael acceptors (for synthesis see the Supporting Information).

Unfortunately, the synthesized inhibitors showed significantly diminished binding affinities compared to their related reversible analogues (Table 6). The ineffectiveness of these inhibitors can be explained by considering the orientation of the thiol function of Cys56. Although PDEδ is very flexible, different co-crystal structures suggest that the thiol points out of the pocket, and thus is not exposed to inhibitors in the binding site (Figure 7 b).

Conclusions and Outlook

We have described the structure-guided development of novel K-Ras–PDEδ inhibitor chemotypes based on pyrrolopyridazi-
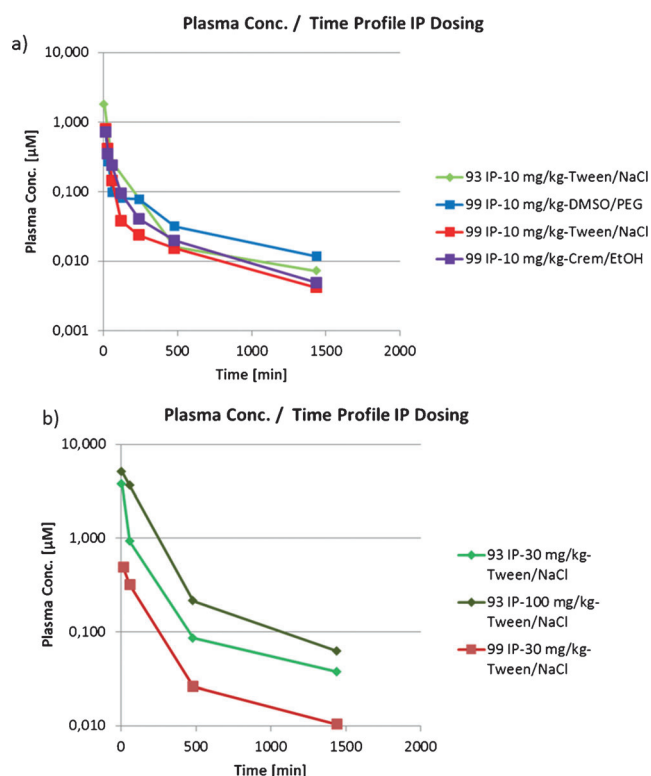
Figure 5. Plasma concentration/time profiles of pyrazolopyridazinone derivatives. Compounds **93** and **99** were administered intraperitoneally (IP) at various doses and in different formulations as indicated. Blood samples were taken over a period of 24 h and analyzed for the total compound concentrations in plasma. All animal work was conducted according to German national guidelines for animal care. Permissions for the conduct of the animal experiments were granted by the Regierungspräsident in Tübingen, Germany.
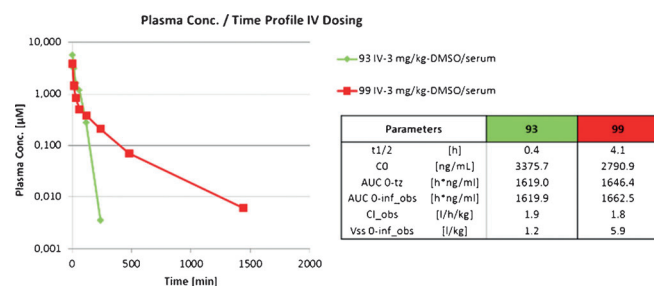
Figure 6. PK profiling of pyrazolopyridazinones. Compounds **93** and **99** were administered to NMRI mice IV at a dose of 3 mg kg^{-1} each. Blood samples were taken over a period of 24 h and analyzed for the total compound concentrations in plasma. Left panel: plasma concentration–time profile over 24 h for **93** and **99**. Right panel: comparison of PK parameters of **93** and **99** calculated from the measured total plasma concentrations. All animal work was conducted according to German national guidelines for animal care. Permissions for the conduct of the animal experiments were granted by the Regierungspräsident in Tübingen, Germany.

none and pyrazolopyridazinone scaffolds, which bind to the farnesyl binding pocket of PDEδ with low nanomolar affinity. Structure–property relationship, in vivo pharmacokinetic (PK) and toxicokinetic (Tox) studies on pyrazolopyridazinone-based K-Ras–PDEδ inhibitors revealed a candidate which may be fur-
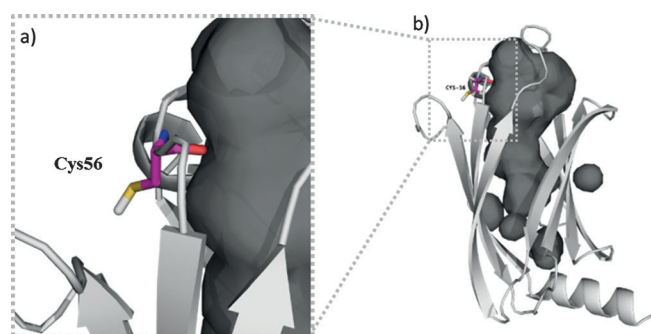

Figure 7. a) Orientation of thiol function of Cys56 showing that it points away from the inhibitor (PDB ID: 5E80). b) Crystal structure of PDEδ highlighting the Cys56 moiety. The pocket surface is shown in dark grey.

Table 6. Binding affinities of pyrrolo- and pyrazolo-derivatives featuring Michael-acceptor functionalities.

Entry	Nr.	R^1	R^2	K_D [nm]
1	**104**			$> 10^3$
2	**105**			$> 10^3$
3	**106**			200 ± 101
4	**107**			$> 10^3$

ther developed for possible in vivo studies employing mouse models.

Acknowledgements

[1] L. Brunsveld, J. Kuhlmann, K. Alexandrov, A. Wittinghofer, R. S. Goody, H. Waldmann, *Angew. Chem. Int. Ed.* **2006**, *45*, 6622–6646; *Angew. Chem.* **2006**, *118*, 6774–6798.

↖↖ These are not the final page numbers!

[2] M. H. Gelb, L. Brunsveld, C. A. Hrycyna, S. Michaelis, F. Tamanoi, W. C. Van Voorhis, H. Waldmann, *Nat. Chem. Biol.* **2006**, *2*, 518 – 528.

[3] J. L. Bos, *Cancer Res.* **1989**, *49*, 4682 – 4689.

[4] J. Downward, *Nat. Rev. Cancer* **2003**, *3*, 11 – 22.

[5] J. S. Sebolt-Leopold, R. Herrera, *Nat. Rev. Cancer* **2004**, *4*, 937 – 947.

[6] P. J. Roberts, C. J. Der, *Oncogene* **2007**, *26*, 3291 – 3310.

[7] A. D. Cox, S. W. Fesik, A. C. Kimmelman, J. Luo, C. J. Der, *Nat. Rev. Drug Discovery* **2014**, *13*, 828 – 851.

[8] N. Berndt, A. D. Hamilton, S. M. Sebti, *Nat. Rev. Cancer* **2011**, *11*, 775 – 791.

[9] D. Vigil, J. Cherfils, K. L. Rossman, C. J. Der, *Nat. Rev. Cancer* **2010**, *10*, 842 – 857.

[10] A. Patgiri, K. K. Yadav, P. S. Arora, D. Bar-Sagi, *Nat. Chem. Biol.* **2011**, *7*, 585 – 587.

[11] T. Maurer, L. S. Garrenton, A. Oh, K. Pitts, D. J. Anderson, N. J. Skelton, B. P. Fauber, B. Pan, S. Malek, D. Stokoe, M. J. C. Ludlam, K. K. Bowman, J. Wu, A. M. Giannetti, M. A. Starovasnik, I. Mellman, P. K. Jackson, J. Rudolph, W. Wang, G. Fang, *Proc. Natl. Acad. Sci. USA* **2012**, *109*, 5299 – 5304.

[12] Q. Sun, J. P. Burke, J. Phan, M. C. Burns, E. T. Olejniczak, A. G. Waterson, T. Lee, O. W. Rossanese, S. W. Fesik, *Angew. Chem. Int. Ed.* **2012**, *51*, 6140 – 6143; *Angew. Chem.* **2012**, *124*, 6244 – 6247.

[13] J. M. Ostrem, U. Peters, M. L. Sos, J. A. Wells, K. M. Shokat, *Nature* **2013**, *503*, 548 – 551.

[14] M. P. Patricelli, M. R. Janes, L.-S. Li, R. Hansen, U. Peters, L. V. Kessler, Y. Chen, J. M. Kucharski, J. Feng, T. Ely, J. H. Chen, S. J. Firdaus, A. Babbar, P. Ren, Y. Liu, *Cancer Discov.* **2016**, *6*, 316 – 329.

[15] S. M. Lim, K. D. Westover, S. B. Ficarro, R. A. Harrison, H. G. Choi, M. E. Pacold, M. Carrasco, J. Hunter, N. D. Kim, T. Xie, T. Sim, P. A. Jänne, M. Meyerson, J. A. Marto, J. R. Engen, N. S. Gray, *Angew. Chem. Int. Ed.* **2014**, *53*, 199 – 204; *Angew. Chem.* **2014**, *126*, 203 – 208.

[16] O. Rocks, M. Gerauer, N. Vartak, S. Koch, Z.-P. Huang, M. Pechlivanis, J. Kuhlmann, L. Brunsveld, A. Chandra, B. Ellinger, H. Waldmann, P. I. H. Bastiaens, *Cell* **2010**, *141*, 458 – 471.

[17] O. Rocks, A. Peyker, M. Kahms, P. J. Verveer, C. Koerner, M. Lumbierres, J. Kuhlmann, H. Waldmann, A. Wittinghofer, P. I. H. Bastiaens, *Science* **2005**, *307*, 1746 – 1752.

[18] S. A. Ismail, Y.-X. Chen, A. Rusinova, A. Chandra, M. Bierbaum, L. Gremer, G. Triola, H. Waldmann, P. I. H. Bastiaens, A. Wittinghofer, *Nat. Chem. Biol.* **2011**, *7*, 942 – 949.

[19] A. Chandra, H. E. Grecco, V. Pisupati, D. Perera, L. Cassidy, F. Skoulidis, S. A. Ismail, C. Hedberg, M. Hanzal-Bayer, A. R. Venkitaraman, A. Wittinghofer, P. I. H. Bastiaens, *Nat. Cell Biol.* **2011**, *14*, 148 – 158.

[20] H. Zhang, X. H. Liu, K. Zhang, C.-K. Chen, J. M. Frederick, G. D. Prestwich, W. Baehr, *J. Biol. Chem.* **2004**, *279*, 407 – 413.

[21] M. Schmick, N. Vartak, B. Papke, M. Kovacevic, D. C. Truxius, L. Rossmannek, P. I. H. Bastiaens, *Cell* **2014**, *157*, 459 – 471.

[22] G. Zimmermann, B. Papke, S. Ismail, N. Vartak, A. Chandra, M. Hoffmann, S. A. Hahn, G. Triola, A. Wittinghofer, P. I. H. Bastiaens, H. Waldmann, *Nature* **2013**, *497*, 638 – 642.

[23] B. Papke, S. Murarka, H. A. Vogel, P. Martín-Gago, M. Kovacevic, D. C. Truxius, E. K. Fansa, S. Ismail, G. Zimmermann, K. Heinelt, C. Schultz-Fademrecht, A. Al Saabi, M. Baumann, P. Nussbaumer, A. Wittinghofer, H. Waldmann, P. I. H. Bastiaens, *Nat. Commun.* **2016**, *7*, 11360.

[24] N. A. Meanwell, *J. Med. Chem.* **2011**, *54*, 2529 – 2591.

[25] G.-B. Liang, D. D. Feng, *Tetrahedron Lett.* **1996**, *37*, 6627 – 6630.

[26] P. Stabile, A. Lamonica, A. Ribecai, D. Castoldi, G. Guercio, O. Curcuruto, *Tetrahedron Lett.* **2010**, *51*, 4801 – 4805.

[27] V. S. Matiichuk, M. A. Potopnyk, N. D. Obushak, *Russ. J. Org. Chem.* **2008**, *44*, 1352 – 1361.

[28] C. Abad-Zapatero, J. T. Metz, *Drug Discovery Today* **2005**, *10*, 464 – 469.

[29] J. Singh, R. C. Petter, T. A. Baillie, A. Whitty, *Nat. Rev. Drug Discovery* **2011**, *10*, 307 – 317.

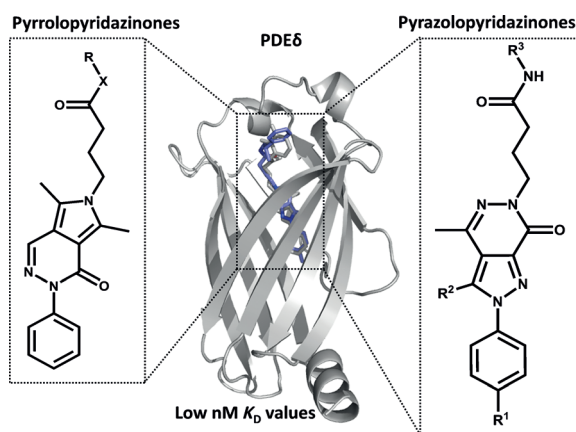These are not the final page numbers! ↗↗

FULL PAPER

■ Chemical Biology

S. Murarka, P. Martín-Gago,
C. Schultz-Fademrecht, A. Al Saabi,
M. Baumann, E. Fansa, S. Ismail,
P. Nussbaumer, A. Wittinghofer,
H. Waldmann*

■■ – ■■

Development of Pyridazinone
Chemotypes Targeting the PDEδ
Prenyl Binding Site

Reaching deep: The identification and structure-guided development of novel K-Ras–PDEδ inhibitor chemotypes based on pyrrolopyridazinones and pyrazolopyridazinones that bind to the farnesyl binding pocket of PDEδ with low nano-molar affinity is described. The results may inspire novel drug-discovery efforts aimed at the development of drugs targeting oncogenic Ras.

↖↖ These are not the final page numbers!